

Article

Characterization, X-ray Absorption Spectroscopic Analysis and Photocatalytic Activity of Co/Zn Co-Doped TiO₂ Nanoparticles Synthesized by One-Step Sonochemical Process

Wanichaya Mekprasart¹, Sorapong Pavasupree², C. K. Jayasankar³, Balaji Rao Ravuri⁴, Chakkaphan Wattanawikkam^{5,*} and Wisanu Pecharapa¹ 

- ¹ College of Materials Innovation and Technology, King Mongkut's Institute of Technology, Ladkrabang, Bangkok 10520, Thailand; wani.mek@gmail.com (W.M.); kpewisan@gmail.com (W.P.)
- ² Department of Materials and Metallurgical Engineering, Faculty of Engineering, Rajamangala University of Technology, Thanyaburi, Pathum Thani 12110, Thailand; sorapong.p@en.rmutt.ac.th
- ³ Department of Physics, Sri Venkateswara University, Tirupati 517502, India; ckjaya@yahoo.com
- ⁴ Department of Physics, School of Science, GITAM Deemed to Be University, Hyderabad 502329, India; balajirao.ravuri@gitam.edu
- ⁵ Division of Physics, Faculty of Science and Technology, Rajamangala University of Technology, Thanyaburi, Pathum Thani 12110, Thailand
- * Correspondence: chakkaphan_w@rmutt.ac.th



Citation: Mekprasart, W.; Pavasupree, S.; Jayasankar, C.K.; Ravuri, B.R.; Wattanawikkam, C.; Pecharapa, W. Characterization, X-ray Absorption Spectroscopic Analysis and Photocatalytic Activity of Co/Zn Co-Doped TiO₂ Nanoparticles Synthesized by One-Step Sonochemical Process. *Crystals* **2021**, *11*, 1254. <https://doi.org/10.3390/cryst11101254>

Academic Editors: Damir Valiev, Jakrapong Kaewkhao, Alessandro Chiasera and Tao Han

Received: 14 July 2021

Accepted: 8 October 2021

Published: 15 October 2021

Publisher's Note: MDPI stays neutral with regard to jurisdictional claims in published maps and institutional affiliations.



Copyright: © 2021 by the authors. Licensee MDPI, Basel, Switzerland. This article is an open access article distributed under the terms and conditions of the Creative Commons Attribution (CC BY) license (<https://creativecommons.org/licenses/by/4.0/>).

Abstract: A novel one-step preparation of sonochemical method was applied to synthesize Co/Zn co-doped TiO₂ nanoparticles using a sonicator of 750 W, 20 kHz for 30 min at room temperature. The formation of the anatase TiO₂ phase for all as-prepared samples was observed from XRD results with a crystalline size in nanoscale. The use of ultrasound allowed for the successful doping of both Co and Zn into the TiO₂ lattice, which was confirmed by Synchrotron light including X-ray near edge structure (XANES) and Extended X-ray absorption fine structure (EXAFS) spectroscopy. Ti K-edge, Co K-edge, and Zn K-edge XANES spectra exhibited the dominating +4, +2, and +2 valence state of Ti, Co, and Zn in as-prepared samples, respectively. A detailed XANES and EXAFS data analysis give strong evidence that the Co/Zn dopants partially replace the Ti atom of the TiO₂ host. The Co/Zn co-doping extends the light absorption of the host to the visible region and restricts the e⁺/h⁺ recombination. The photocatalytic activity of samples was tested for degradation of Rhodamine B dye solution under visible light irradiation. The as-synthesized of the co-doped catalyst was presented as highly efficient, with 2.5 and 5 times dye degradation compared with single-doped and bare TiO₂.

Keywords: Co/Zn co-doped TiO₂; XANES; EXAFS; photocatalyst; sonochemical method

1. Introduction

The development of photo-catalyst materials to inactivate pathogenic in aqueous media, degradation of hazardous materials, environmental cleanup, and the purification of pollution in water and air is a matter of growing interest [1]. Particularly, the use of visible light for driving the photocatalytic activity employing solar light is a great challenge. Of the semiconductor photocatalytic materials, titanium dioxide (TiO₂) has been the most extensively premeditated and utilized in various applications due to high chemical stability, great oxidizing strength, cheapness, and environmental friendliness [2,3]. However, because of the large energy band gap (3.0–3.2 eV for anatase and rutile phase), TiO₂ can only absorb UV light and is limited as a solar light-driven photocatalyst [4]. In addition, TiO₂ has a high recombination rate between the electron (e⁻) and hole (h⁺) pairs which results in low quantum yield. Hence, in order to enhance the visible light absorption and to slow down the e⁻/h⁺ recombination, one of the approaches is to dope with metal/nonmetal, such as Zn, Mn, Co, Fe, Ni, Cu, V, Cr, Mo, Ce, Zr, Au, Y, F, N, I [5–19]

and so on. Moreover, recent reports are focused on co-doping of TiO₂ photocatalysts with different ions (metal/metal and metal/nonmetal), allowing better separation of the photogenerated electron and holes, assuring an effective enhancement of visible light adsorption together with higher photocatalytic activity [20–22]. Among various metal ions, 3d-transition metals ions such as Zn²⁺ and Co²⁺ are considered to be the candidate dopants, which the radii ions are similar, and the electronegativity ions are considerably approximate. So, the Co and Zn can enter the lattice of TiO₂ resulting in the improvement of the visible light harvesting and act as the trap for e⁻/h⁺ pairs resulting in the enhance of charge carrier separation. In the report by J. Cai et al., highly efficient degradation of organic pollutants was presented by the stable boron and cobalt co-doped TiO₂ nanotubes [23]. Photocatalytic degradation of opaque dye acid fuchsin by Pr-Co co-doped TiO₂ was reported by J. Yu [24]. Additionally, detailed atomistic knowledge and local structure are the most important for the understanding of materials functions. X-ray absorption spectroscopy (XAS) is a more specialized technique to examine the local atomic, electronic structure, atomic geometry, and site/symmetry selected density of unoccupied electronic states [25,26]. Many researchers have worked on the development of TiO₂-based nanoparticles, but most of the work involves the fabrication of nanostructures using conventional methods, these methods providing time-consuming and costly procedures. The facile and clean synthesis using ultrasounds has been confirmed to be useful for fabricating nanostructured materials, with fine dispersion and size reduction of particles. In addition, it prevents agglomeration and uniformly distributes particles [27]. The cavities are created in the solution due to the ultrasonic irradiation, then the cavities collapse after reaching a certain size releasing a large magnitude of energy. Under harsh conditions, various physical changes and reactions occur. So, various nanostructure materials can be successfully formed with desired nanosized. In previous work, we have reported the use of the sonochemical method to prepare nanomaterials at room temperature, such as Mn-Zn co-doped TiO₂ nanoparticles [28], perovskite ZnTiO₃ nanoparticles [29], and Co and Mn-doped ZnTiO₃ nanoparticles [30].

Hence, the present study aimed to investigate the fabrication of Co/Zn co-doped TiO₂ nanoparticles via facile one-step of the sonochemical method. The effect of dopant ions on structural phase, morphology, chemical composition, and optical properties were examined. The local structure of prepared samples was characterized by X-ray absorption near-edge structure and extended X-ray absorption fine structure technique. Rhodamine B dye was considered as a model pollutant to study the photocatalytic degradation capability of the synthesized nanoparticles under visible light irradiation.

2. Materials and Methods

Titanium isopropoxide (C₁₂H₂₈O₄Ti), zinc nitrate hexahydrate (Zn(NO₃)₂·6H₂O), and cobalt nitrate hexahydrate (Co(NO₃)₂·6H₂O) purchased from Aldrich were used as Ti, Zn and Co precursors, respectively. The molar ratio of Zn dopant was fixed to 1 mol% and varying the Co concentration at 1, 2, 3, and 5 mol%. First, 0.05 M titanium isopropoxide was dissolved in absolute ethanol and zinc nitrate was then added to the solution under a magnetic stirrer for 20 min. After that, the Co at different concentrations was added to the solution followed by DI water. The mixing solution was kept under stirring for 15 min. Finally, the mixed precursor was irradiated under a high ultrasonic sonicator (750 W, 20 kHz) for 30 min at room temperature together with the slow addition of NaOH solution (6g of NaOH pallet in 20 mL of DI) until the precipitation solution was obtained. The obtained solution was washed thoroughly with deionized water until the pH became 7 and then dried at 120 °C for 12 h. Finally, as-synthesized TiO₂ nanopowders were obtained.

Phase structure of as-synthesized samples was characterized by the X-ray diffraction technique (XRD). Surface morphology and particles size analysis were obtained by the Schottky field emission scanning electron microscope (FESEM) model: SU8230. The UV-visible diffused reflection spectroscopy (UV-vis DRS) model: Perkin Elmer model Lambda 750s was used to study the optical properties of all samples. The chemical composition

of samples was obtained by the X-ray absorption spectroscopy (XAS) technique at Ti, Zn, and Co K-edge using Beamline-8, Synchrotron Light Research Institute (SLRI) Thailand, with the storage ring running at 1.2 GeV and beam current of beam current 80–120 mA. The data collection was carried out in transmission mode for Ti K-edge (at 4966 eV) and fluorescent mode for Zn K-edge (9659 eV) and Co K-edge (7709 eV) using double crystal Ge(220) monochromator. ATHENA and ATHEMIS programs were used for all XAS analyses. The specific area of prepared samples was measured by the surface area and pore size analyzer, Quantachrome, model: Autosorb iQ-C-XR. The photocatalytic behavior of prepared samples was evaluated using RhB degradation as a test reaction. In a typical, the photocatalytic performance was evaluated by the degradation of Rhodamine B (0.01 mmol) dye in an aqueous solution under visible light irradiation. The 0.08 g of catalyst was added to 100 mL of dye solution, the suspension was stirred for 20 min in the dark to ensure the establishment of adsorption/desorption between dye and catalyst, and then the visible light was irradiated. During the photocatalytic reaction, 4 mL of dye solution was taken at selected time intervals. The concentration of RhB in the supernatants was measured by UV-vis spectroscopy at a wavelength of 554 nm.

3. Results

3.1. Phase Structure

The crystallographic structures of as-synthesized pure TiO₂, single-doping, and co-doping nanopowders prepared by the single-step sonochemical method were confirmed by XRD investigation as seen in Figure 1. The diffraction position of 2θ at 25.3°, 37.6°, 48.1°, and 54.1° corresponded to the (101), (112), (200), and (105) crystallographic planes of the anatase-TiO₂ phase, respectively. All XRD diffractograms of co-doping samples clearly exhibit the formation of pure anatase TiO₂ phase without any secondary phase of metal oxide. By the increase in the cobalt content in TiO₂ samples, the intensities of the main anatase phase slightly declined, and the width of diffraction peaks of 101 became broader, clearly representing the reduction of the crystalline size. These may have indicated the shrinkage of some of the TiO₂ lattices caused by the incorporation of the doped Co/Zn ions. From the results, it can be proposed the sonochemical reaction mechanism that the hydrolytic species of TTIP in water condensed to form a large number of tiny gel nuclei, which aggregated to form larger clusters. Ultrasonic irradiation from the sonicator generates a lot of local hot spots within the solution, outside which the polycondensation of ≡Ti–OH or ≡Ti–OR is promoted [31]. The local hot spot is an important role in the rapid loss of organic residue and water. This further causes the formation of a large number of seed nuclei, which leads to smaller grain size. In this case, the preferred region for TiO₂ crystallization is the interfacial zone of the ultrasound cavity, which is due to the low vapor pressure of the reactants. Compared with the traditional stirring technology, sonochemistry has been demonstrated to stimulate the speed of the reaction in liquid. Hence, high intensity of ultrasounds can accelerate the crystallization of TiO₂, and nanocrystalline products were obtained without the heat-treatment process.

3.2. Structural Study

The XAS technique with synchrotron light including X-ray absorption near edge structure (XANES) and extended X-ray absorption fine structure (EXAFS) was used to investigate the electronic nature of Co/Zn co-doped TiO₂ samples. The normalized XANES spectra of single-doped, co-doped TiO₂ and the reference standards are shown in Figure 2. Generally, the interpretation of Ti K-edge is intricate, of which the main features of post-edge edge (>4980 eV) can be determined to dipole transition from Ti 1s → 4p states, whereas the pre-edge (<4980 eV) can be assigned to the electronic transition to the crystal field split hybridized states between Ti 4p and 3d orbital based on a mixture of quadrupole and dipole excitations [6]. By examining these data and comparing with the literature, as displayed in Figure 2a, the Ti K-edge for TiO₂, single-doping, and co-doping samples describes the pre-edge spectra of anatase TiO₂ based specimens including four characteristic spectra

denoted as A_1 , A_2 , A_3 , and B in the energy region of 4988–4996 eV. The pre-edge Ti K-edge XANES structure arises from 1s to 4d dipole electric transition, with the intensities of the peaks affected by the local geometry and particular medium-range structure of the sample around central Ti atoms [6]. Moreover, the features of pre-edge such as height and position indicate that these samples contain hexa-coordinated Ti^{4+} atoms. The partial split of pre-edge spectra of Ti K-edge could be observed in the first derivative XANES as written in Figure 2b, representing the edge raising of structures, which has been discussed above.

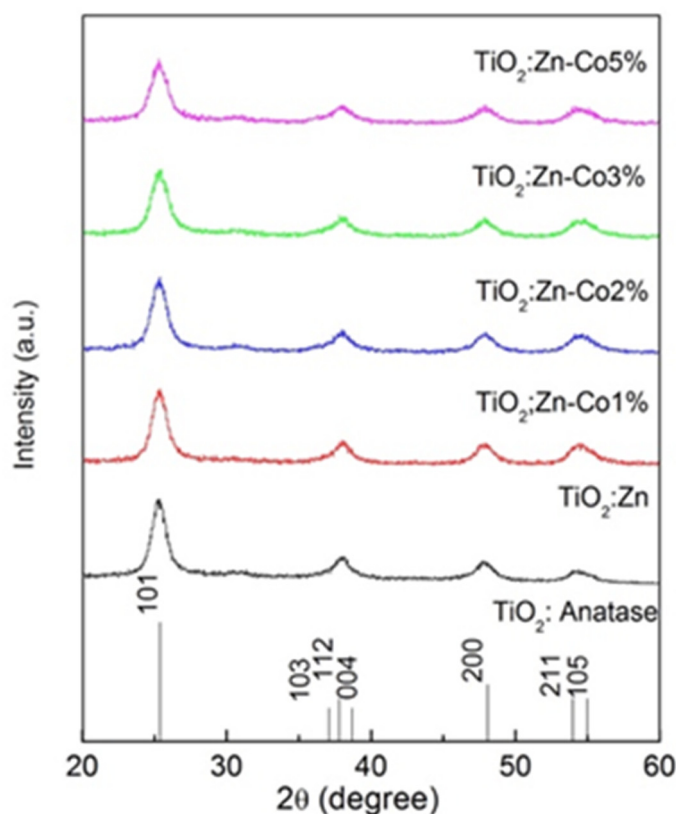


Figure 1. Powder XRD pattern of Zn-TiO₂, Co/Zn co-doped TiO₂ nanoparticles.

To confirm the existence of Co and Zn dopants ions in TiO₂ lattice, Co- and Zn K-edge XANES measurements were conducted. For the Zn K-edge, the normalized XANES spectra and the first derivative of prepared samples and ZnO reference standard are shown in Figure 2c,d, respectively. Following the inspection of the spectra, it was found that the spectra exhibit a strong absorption edge in a range of 9660–9670 eV with no pre-edge region because the 3d orbital in Zn²⁺ ion is fully occupied by electrons. The energy absorption spectra of all samples correspond to the Zn²⁺ of the ZnO reference standard. Thus, the Zn species being introduced into the TiO₂ host is evidently present in a 2+ oxidation state. In the case of Co K-edge, as seen in Figure 2e,f, normalized XANES spectra and their first derivative of all as-prepared samples reveals the main absorption energy at ~7710 eV corresponding to the transition to higher energy levels. The strong absorption edge of the co-doped sample corresponds to the CoO reference standard. It can be concluded that prepared samples comprise Co 2+ of oxidation state. Moreover, both post-edge spectra of Zn K-edge (after 9670 eV) and Co K-edge (after 7730 eV) are not likely to occur ZnO and CoO standard spectrum, respectively, which is presumed the Zn²⁺ and Co²⁺ cations partially replaced Ti⁴⁺ cations to octahedrally coordinated with six oxygen anions. However, the Co-dopants do not exhibit the changing in pre- and post-edge of XANES feature, this implies that the dopant ion might not change the host structure but be incorporated in the TiO₂ host.

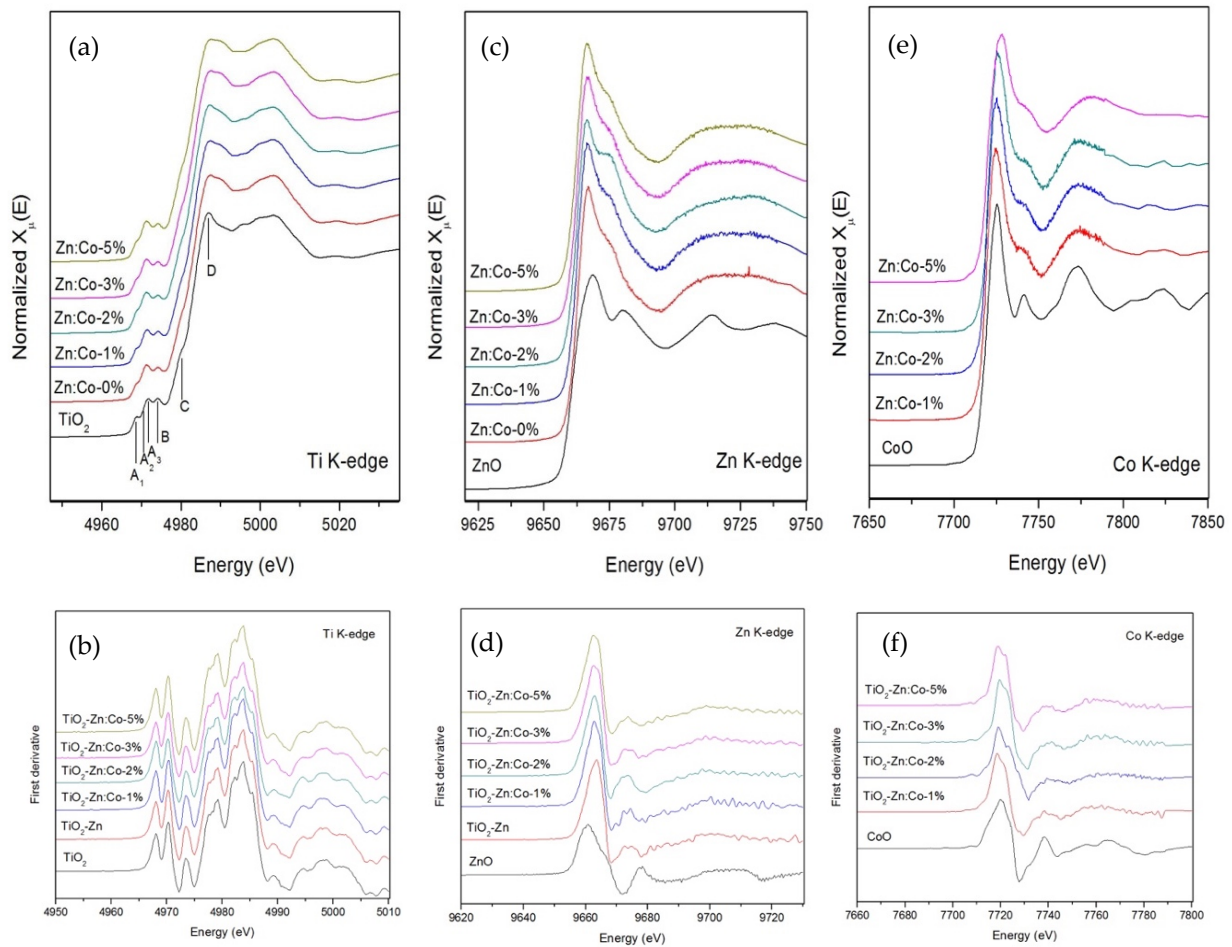


Figure 2. Normalized XANES spectra and first derivative XANES of Co/Zn co-doped TiO₂: (a,b) Ti K-edge, (c,d) Zn K-edge, and (e,f) Co K-edge.

For an in-depth elucidation of the local structure in as-prepared samples, the EXAFS inquiry was employed at Ti K-edge, Zn K-edge, and Co K-edge. EXAFS spectra are Fourier-transformed (FT) with k^2 -weighting to produce radial distribution functions, as shown in Figure 3. By analysis of Ti as an absorber atom for TiO₂, there are two peaks appearing at around 1.9 Å and 2.7 Å (Black line). The first peak is the Ti-O coordination, associating with the single scattering path of absorbing Ti atom with the nearest neighboring O atoms by six-coordinated around the Ti atom. While the second peak is the Co/Zn-Ti coordination assigned to the single and multiple scattering paths of the absorbing Ti atom with the nearest neighboring Ti atoms and with the nearest neighboring Co/Zn atoms. For describing the environment around Zn- and Co-dopants ions, FT spectra of co-doped samples at Zn and Co were analyzed. It can be seen that the radial distribution features for the Zn/Co dopants in all TiO₂ samples studied are similar to the Ti in TiO₂. This indicates that the environment around dopant ions is identical with the host Ti, which can be implied the Zn/Co dopants replaced in the Ti site of samples.

3.3. Morphology and Surface Area Analysis

The FESEM images of single-doped and co-doped samples are displayed in Figure 4. As shown in Figure 4a, almost spherical-shaped particles with particle agglomeration were observed in the single Zn doped TiO₂ samples. For 3% and 5% co-doping samples (Figure 4b,c), FESEM images exhibit the uniform distribution of nanoparticles, especially the Co-3%, as seen in Figure 4b. In addition, the micrograph in Figure 4d demonstrated that the particle size analysis by FESEM image, the average particle sizes are around 10–20 nm.

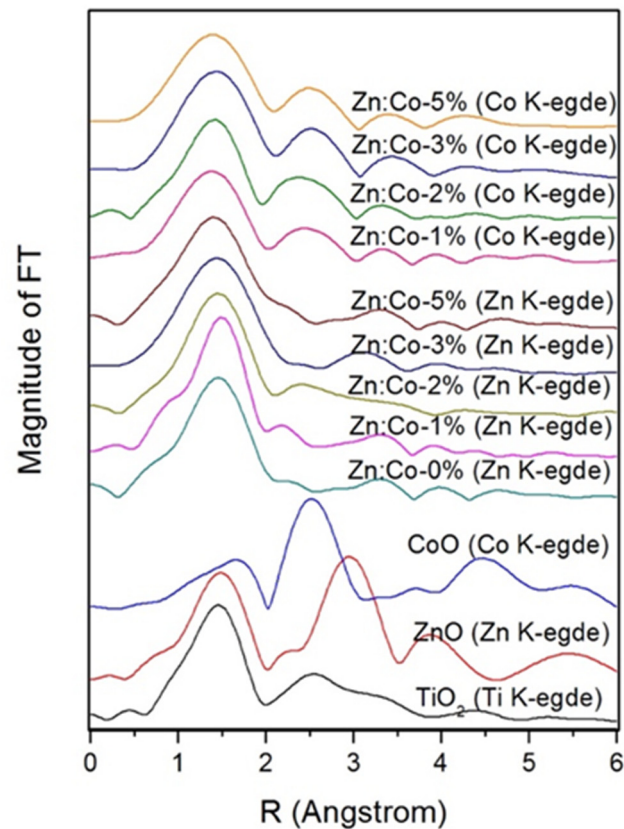


Figure 3. Fourier transform magnitudes of EXAFS spectra of k^2 -weighted data for Co/Zn co-doped TiO_2 with their reference standard at Ti, Zn, and Co K-edge.

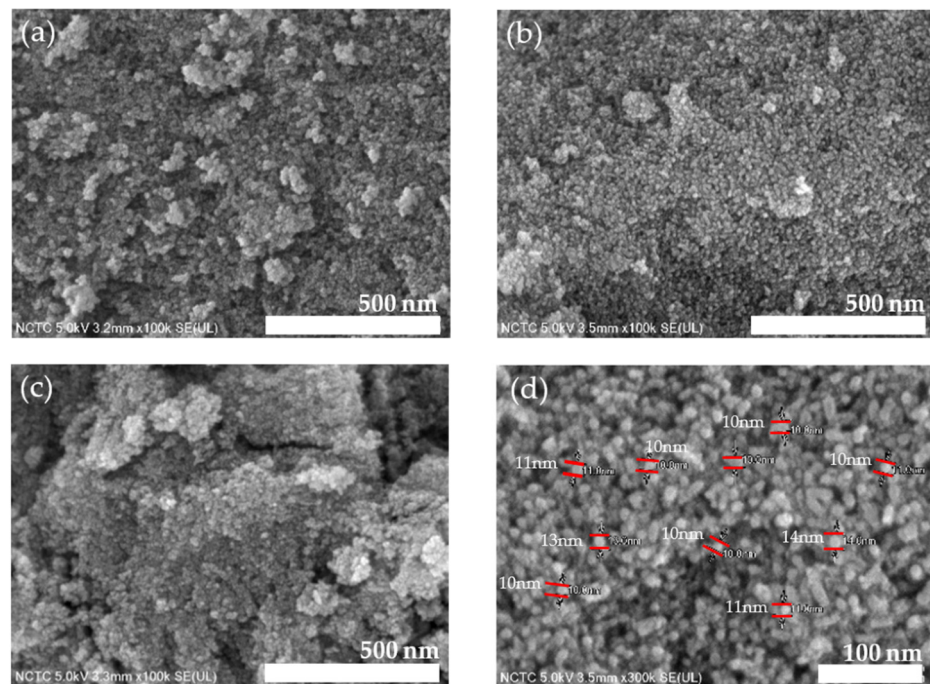


Figure 4. FESEM images of (a) TiO_2 -Zn-1%, (b) TiO_2 -Zn/Co-3%, (c) TiO_2 -Zn/Co-5% and (d) particle size analysis of TiO_2 -Zn/Co-3%.

For the specific area of all as-prepared samples, N_2 adsorption-desorption and corresponding pore size distribution calculated by BJH (TiO_2 -Zn/Co-3%) are shown in

Figure 5a,b, respectively. It can be seen that the single- and co-doping shows isotherm of type II, which is a typical medium microporous structure. The surface area of Zn-TiO₂, 1%-Co/Zn-TiO₂, 3%-Co/Zn-TiO₂, and 5%-Co/Zn-TiO₂ are 190.86, 201.77, 205.27, 206.40, 208.83 m²/g, respectively. The large surface of co-doped samples compared to pure-, single-doped, and previous studies may increase the interaction in photocatalytic activity, which is beneficial for photo photocatalytic efficiency.

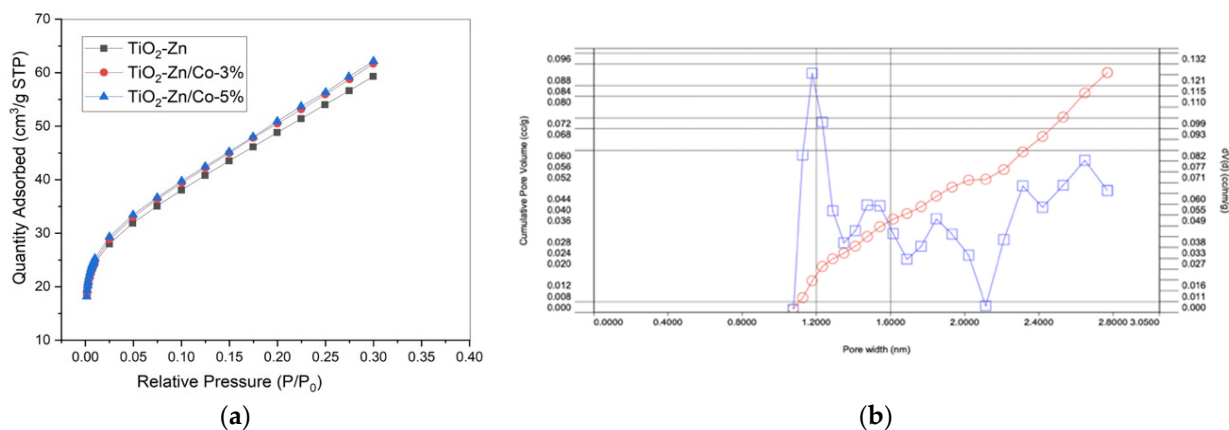


Figure 5. (a) Nitrogen sorption isotherms of the as-synthesized single-doped TiO₂ and Zn/Co co-doped TiO₂ and (b) pore diameter distribution curve TiO₂-Zn/Co-3%.

3.4. Optical Properties

The UV-vis DRS measurement of pure TiO₂, single-doped, and co-doped samples is shown in Figure 6. For the single-doped samples, extended visible light absorption is observed compared to pure TiO₂. Furthermore, the larger absorption in the visible region is noticed in the co-doped samples. It is suggested that increasing co-dopant concentration could result in the reduction of bandgap energy and the enhancement in visible light-harvesting of TiO₂. This feature would be correlated to the incorporation of dopant ions in the host lattice that could generate new electronic states in the TiO₂ bandgap. Hence the distance of charge transfers between the *d* electron of the dopant ion and the conduction or valence band is narrowed, leading to the increase in visible light response of the material. Moreover, the different valence states of dopants including Co²⁺ and Zn²⁺ from the host matrix Ti⁴⁺ may induce the substantial generation of oxygen deficiencies. The bandgap energies of all samples were calculated from the DRS spectra employing a modified Kubelka-Munk equation as plotted in Figure 6b. It is obviously noticed that the deposition of co-dopants significantly affects the decrease of the bandgap energy of the host TiO₂ which has an estimated value of 3.21, 3.01, 2.78, 2.75, 2.72, and 2.68 eV for pure TiO₂, Zn-TiO₂, 1%Co/Zn-TiO₂, 3%Co/Zn-TiO₂, and 5%Co/Zn-TiO₂, respectively. From these results, it was inferred that the Co/Zn co-doped TiO₂ could be activated effectively under visible light illumination.

3.5. Photocatalytic Activity

The photocatalytic performance of the prepared samples was employed for rhodamine b dye decolorization under visible light irradiation. Pure RhB exhibit the absorption band at 544 nm, which is assigned to the chromophoric group. The percentage of degradation (*D*) for RhB dye was calculated using the following equation;

$$D = \frac{[A_0 - A_t]}{A_0} \times 100\% \quad (1)$$

where *A*₀ is the absorbance value of the initial RhB solution, *A*_{*t*} is the absorbance value of degraded RhB solution at the reaction time *t*. Under the visible light irradiation without the

catalyst, no decrease in the RhB concentration is observed, implying that the self-photolysis of RhB is negligible when irradiated with visible light. When the reaction was carried out by a single doped sample, around 40% of RhB degradation after 90 min was obtained as seen in Figure 6. For the Co/Zn co-doped TiO_2 (Figure 7a), the superior degradation of around 80% was found in the samples containing 3% of Co-content after 90 min of irradiation time while the sample with 1, 2, and 5% Co doping content exhibited about 51, 73 and 71% of photodecolorization, respectively. According to the results, all as-synthesized co-doped catalysts show higher degradation rates than Co- and Zn- single-doped and bare TiO_2 . Obviously, a comparison in the plots of dye degradation shows that the concentration of as-prepared catalyst can indeed influence the degradation efficiency. The increase of dopant content to 3 mol% resulted in the increase in dye degradation, which might be attributed to the Co increased, the surface barrier becomes higher and narrower space charge obtained, leading to easy of e/h pairs. However, a slight decrease of dye decomposition was observed when the concentration of Co-doped was further increased to 5mol%, this may be due to when the content of cobalt dopant is increased beyond the limit, the space charge recombination is lower and penetration depth of light into the catalyst greatly exceeds the layer of space charge, indicating in high recombination of e/h pairs [32].

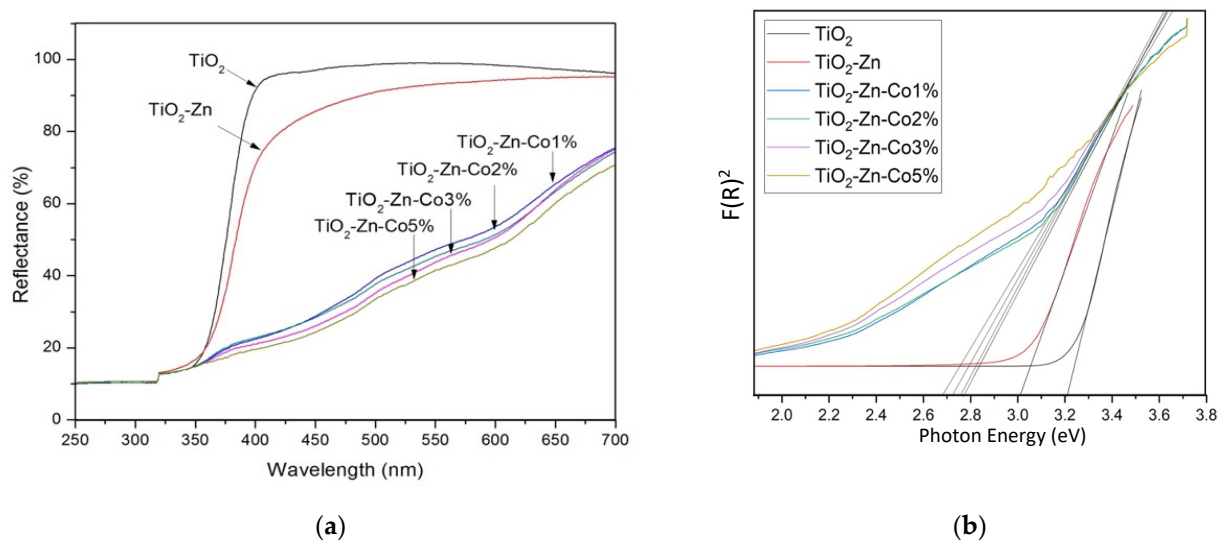


Figure 6. (a) UV-vis diffuse reflectance spectra and (b) Energy band gap of Co/Zn co-doped TiO_2 .

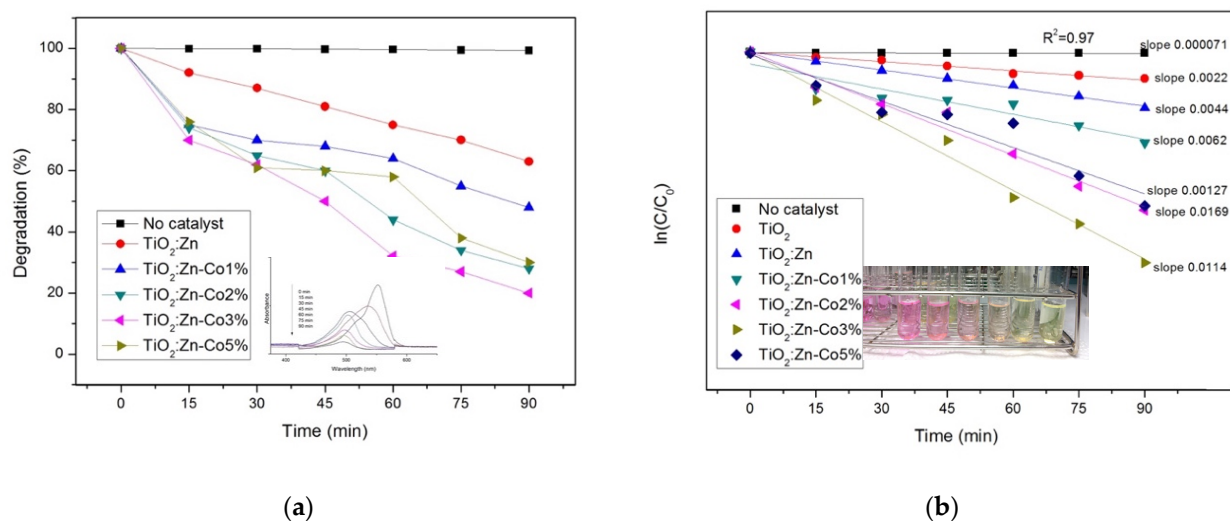


Figure 7. (a) Photocatalytic degradation curves with time independence UV-vis and (b) kinetic linear fitting curves for Co/Zn co-doped TiO_2 catalyst under visible light irradiation in the presence of RhB dye.

Reaction kinetics gives information about the reaction rates and the mechanisms by which the reactants are converted to the products. The equation for pseudo-first-order kinetic is given below;

$$- \ln \left(\frac{C}{C_0} \right) = kt \quad (2)$$

where C and C_0 are the final and initial concentrations (ppm) of RhB, k is the apparent reaction rate constant (min^{-1}) and t is the irradiation time (min). Figure 7b demonstrates the photocatalytic reaction kinetic of RhB degradation in the solution based on the data plotted in Figure 6. As it can be seen, a rather good correlation to pseudo-first-order reaction kinetics ($R^2 = 0.97$) was found, which suggests that the RhB degradation over these samples follows the first-order kinetics. Among all as-prepared catalysts, 3% of Co/Zn doped TiO_2 shows the highest reaction rate constant of 0.0114 min^{-1} , which is about 5.2 and 2.6 times that over pure and single-doping catalysts, respectively.

It is observed that the superior performance of organic compounds photodegradation was found in Co/Zn co-doping TiO_2 . It may be due to many factors, such as the increase of visible light harvesting due to the narrowing energy band gap, slower time for e^-/h^+ pairs recombination, and greater hydroxyl radical generation. Additionally, the possible mechanism of photodegradation for organics compounds using metal-doped TiO_2 was studied by comparing with similarly reported [33–36]. They reported that when the light irradiation on the metal-doped TiO_2 catalyst, photoexcited electrons were transferred from the valence band to newly created electronic states in the band structure via metals incorporated into the TiO_2 matrix. Then, the transferred electron reacted with an oxygen molecule (O_2) to generate a superoxide anion ($\cdot\text{O}_2^-$); $e^- + \text{O}_2 \rightarrow \cdot\text{O}_2^-$, and a positive hole in the valence band of TiO_2 reacted with (i) a water molecule (H_2O) or (ii) hydroxyl ion (OH^-) to form a hydroxyl radical ($\cdot\text{OH}$); (i) $h^+ + \text{H}_2\text{O} \rightarrow \cdot\text{OH} + \text{H}^+$ and (ii) $h^+ + \text{OH}^- \rightarrow \cdot\text{OH}$. Finally, the reactive species $\cdot\text{O}_2^-$ and $\cdot\text{OH}$ could oxidize the target organic compounds to generate CO_2 , CO, and other byproducts.

4. Conclusions

In summary, Co/Zn co-doped TiO_2 was successfully synthesized by a facile one-step sonochemical method at room temperature. The use of ultrasounds allowed for the successful doping of both Co and Zn into the TiO_2 lattice, which caused a shift in the light absorption toward the higher wavelength. XANES measurement confirmed the oxidation state of 4+, 2+, and 2+ for Ti, Zn, and Co, respectively. EXAFS analysis reveals that the cobalt and zinc are possibly occupied into TiO_2 lattice, by replacing some Ti^{4+} . The Co/Zn co-doped TiO_2 photocatalyst exhibited good photodegradation of RhB dye under visible light irradiation. The best decolorization performance was achieved in the content of 3% for cobalt doping concentration. It is presumed that (i) the sonochemical method provides the small nanoparticles resulting in higher surface area and (ii) the incorporation of Co and Zn lead to enhance visible light harvesting and to diminish the electron-hole recombination, which improved the photocatalytic behavior.

Author Contributions: Conceptualization, C.W., W.M., S.P. and W.P.; methodology, W.M., S.P. and C.W.; software, C.W.; validation, W.P., S.P. and C.K.J.; formal analysis, C.W., W.P., S.P. and B.R.R.; investigation, C.W. and S.P.; resources, W.P. and S.P.; data curation, W.M.; writing—original draft preparation, C.W., W.M. and S.P.; writing—review and editing, W.P., C.K.J. and S.P.; visualization, C.W.; supervision, W.P.; project administration, W.P.; funding acquisition, S.P. and W.P.. All authors have read and agreed to the published version of the manuscript.

Funding: This research was funded by Fundamental Research Budget Allocation (RFB630004/0168) grant funded by Thailand Science Research and Innovation (TSRI) (Granted No. IRF63A0704A.4).

Data Availability Statement: Not applicable.

Acknowledgments: Authors would like to thank the Division of Physics, Faculty of Science and Technology, Rajamangala University of Technology Thanyaburi (RMUTT), College of Materials Innovation and Technology, King Mongkut's Institute of Technology Ladkrabang (KMUTL), and Smart Materials Research Unit (SMRU) for supporting the facilities. Authors gratefully acknowledge BL-8 at Synchrotron Light Research Institute (SLRI), Nakhon Ratchasima, Thailand, for XAS measurement.

Conflicts of Interest: The authors declare no conflict of interest.

References

1. Bhatkhande, D.S.; Pangarkar, V.G.; Beenackers, A.A.C.M. Photocatalytic degradation for environmental applications—A review. *J. Chem. Technol. Biotechnol.* **2001**, *77*, 102–116. [[CrossRef](#)]
2. Rajeshwar, K.; Chenthamarakshan, C.R.; Goeringer, S.; Djukic, M. Titania-based heterogeneous photocatalysis. Materials, mechanistic issues, and implications for environmental remediation. *Pure Appl. Chem.* **2001**, *73*, 1849–1860. [[CrossRef](#)]
3. Nakata, K.; Fujishima, A. TiO₂ photocatalysis: Design and applications. *J. Photochem. Photobiol. C Photochem. Rev.* **2012**, *13*, 169–189. [[CrossRef](#)]
4. Anpo, M.; Takeuchi, M. The design and development of highly reactive titanium oxide photocatalysts operating under visible light irradiation. *J. Catal.* **2003**, *216*, 505–516. [[CrossRef](#)]
5. Hernández, J.V.; Coste, S.; Murillo, A.G.; Romo, F.C.; Kassiba, A. Effects of metal doping (Cu, Ag, Eu) on the electronic and optical behavior of nanostructured TiO₂. *J. Alloy Compd.* **2017**, *710*, 355–363. [[CrossRef](#)]
6. Jaihindh, D.P.; Verma, A.; Chen, C.-C.; Huang, Y.-C.; Dong, C.-L.; Fu, Y.-P. Study of oxidation states of Fe- and Co-doped TiO₂ photocatalytic energy materials and their visible-light-driven photocatalytic behavior. *Int. J. Hydrogen Energy* **2019**, *44*, 15892–15906. [[CrossRef](#)]
7. Wattanawikkam, C.; Pecharapa, W.; Ishihara, K.N. X-ray absorption spectroscopy analysis and magnetic properties of M-doped TiO₂ nanoparticles (M=Co, Mn, Ni and Zn) prepared by co-precipitation method. *Ceram. Int.* **2017**, *43*, S397–S402. [[CrossRef](#)]
8. Chen, W.-T.; Dong, Y.; Yadav, P.; Aughterson, R.D.; Sun-Waterhouse, D.; Waterhouse, G.I. Effect of alcohol sacrificial agent on the performance of Cu/TiO₂ photocatalysts for UV-driven hydrogen production. *Appl. Catal. A Gen.* **2020**, *602*, 117703. [[CrossRef](#)]
9. Noonuruk, R.; Wattanawikkam, C. Visible-light-driven Photodegradation of Commercial Dyes by the Cooperation of Co-doped TiO₂ Material. *Curr. Appl. Sci. Technol.* **2020**, *20*, 43–51. [[CrossRef](#)]
10. Inturi, S.N.R.; Boningari, T.; Suidan, M.; Smirniotis, P.G. Visible-light-induced photodegradation of gas phase acetonitrile using aerosol-made transition metal (V, Cr, Fe, Co, Mn, Mo, Ni, Cu, Y, Ce, and Zr) doped TiO₂. *Appl. Catal. B Environ.* **2014**, *144*, 333–342. [[CrossRef](#)]
11. Kerkez-Kuyumcu, Ö.; Kibar, M.E.; Dayıoğlu, K.; Gedik, F.; Akin, A.N.; Ozkara-Aydinoglu, S. A comparative study for removal of different dyes over M/TiO₂ (M=Cu, Ni, Co, Fe, Mn and Cr) photocatalysts under visible light irradiation. *J. Photochem. Photobiol. A Chem.* **2015**, *311*, 176–185. [[CrossRef](#)]
12. Wattanawikkam, C.; Pecharapa, W. Synthesis and Characterization of Zn-Doped TiO₂ Nanoparticles via Sonochemical Method. *Integr. Ferroelectr.* **2015**, *165*, 167–175. [[CrossRef](#)]
13. Makdee, A.; Unwiset, P.; Chanapathrapol, K.C.; Kidkhunthod, P. Effects of Ce addition on the properties and photocatalytic activity of TiO₂, investigated by X-ray absorption spectroscopy. *Mater. Chem. Phys.* **2018**, *213*, 431–443. [[CrossRef](#)]
14. Katoueizadeh, E.; Zebajrad, S.M.; Janghorban, K. Synthesis and enhanced visible-light activity of N-doped TiO₂ nano-additives applied over cotton textiles. *J. Mater. Res. Technol.* **2018**, *7*, 204–211. [[CrossRef](#)]
15. Kahattha, C.; Wongpisutpaisan, N.; Vittayakorn, N.; Pecharapa, W. Physical properties of V-doped TiO₂ nanoparticles synthesized by sonochemical-assisted process. *Ceram. Int.* **2013**, *39*, S389–S393. [[CrossRef](#)]
16. Wang, Q.; Rhimi, B.; Wang, H.; Wang, C. Efficient photocatalytic degradation of gaseous toluene over F-doped TiO₂/exfoliated bentonite. *Appl. Surf. Sci.* **2020**, *530*, 147286. [[CrossRef](#)]
17. Suwannaruang, T.; Kidkhunthod, P.; Chanlek, N.; Soontaranon, S.; Wantala, K. High anatase purity of nitrogen-doped TiO₂ nanorice particles for the photocatalytic treatment activity of pharmaceutical wastewater. *Appl. Surf. Sci.* **2019**, *478*, 1–14. [[CrossRef](#)]
18. Saroj, S.; Singh, L.; Singh, S.V. Solution-combustion synthesis of anion (iodine) doped TiO₂ nanoparticles for photocatalytic degradation of Direct Blue 199 dye and regeneration of used photocatalyst. *J. Photochem. Photobiol. A Chem.* **2020**, *396*, 112532. [[CrossRef](#)]
19. Gordon, W.; Balboa, A.; Giles, S.; Epshteyn, A.; Ávalos-Ovando, O.; Govorov, A.; McEntee, M.; Baturina, O. Visible Light-Induced Reactivity of Plasmonic Gold Nanoparticles Incorporated into TiO₂ Matrix towards 2-Chloroethyl Ethyl Sulfide. *Crystals* **2021**, *11*, 659. [[CrossRef](#)]
20. Siddiqua, A.; Masih, D.; Anjum, D.; Siddiq, M. Cobalt and sulfur co-doped nano-size TiO₂ for photodegradation of various dyes and phenol. *J. Environ. Sci.* **2015**, *37*, 100–109. [[CrossRef](#)]
21. Isari, A.A.; Hayati, F.; Kakavandi, B.; Rostami, M.; Motevassel, M.; Dehghanifard, E. N, Cu co-doped TiO₂@functionalized SWCNT photocatalyst coupled with ultrasound and visible-light: An effective sono-photocatalysis process for pharmaceutical wastewaters treatment. *Chem. Eng. J.* **2020**, *392*, 123685. [[CrossRef](#)]
22. Bramhankar, T.; Pawar, S.; Shaikh, J.; Gunge, V.; Beedri, N.; Baviskar, P.; Pathan, H.; Patil, P.; Kambale, R. Effect of Nickel–Zinc Co-doped TiO₂ blocking layer on performance of DSSCs. *J. Alloy Compd.* **2020**, *817*, 152810. [[CrossRef](#)]

23. Cai, J.; Zhou, M.; Xu, X.; Du, X. Stable boron and cobalt co-doped TiO₂ nanotubes anode for efficient degradation of organic pollutants. *J. Hazard. Mater.* **2020**, *396*, 122723. [[CrossRef](#)]
24. Yu, J.; Zou, J.; Xu, P.; He, Q. Three-dimensional photoelectrocatalytic degradation of the opaque dye acid fuchsin by Pr and Co co-doped TiO₂ particle electrodes. *J. Clean. Prod.* **2020**, *251*, 119744. [[CrossRef](#)]
25. Sharma, A.; Varshney, M.; Shin, H.J.; Lee, B.-H.; Chae, K.H.; Won, S.O. Effect of Cu insertion on structural, local electronic/atomic structure and photocatalyst properties of TiO₂, ZnO and Ni(OH)₂ nanostructures: XANES-EXAFS study. *Mater. Chem. Phys.* **2017**, *191*, 129–144. [[CrossRef](#)]
26. Bootchanont, A.; Rujirawat, S.; Yimnirun, R.; Guo, R.; Bhalla, A. Local structure study of phase transition behavior in Ba(Ti,Sn)O₃ perovskite by X-ray absorption fine structure. *Ceram. Int.* **2016**, *42*, 8151–8154. [[CrossRef](#)]
27. Yadav, R.S.; Mishra, P.; Pandey, A.C. Growth mechanism and optical property of ZnO nanoparticles synthesized by sonochemical method. *Ultrason. Sonochemistry* **2008**, *15*, 863–868. [[CrossRef](#)]
28. Wattanawikkam, C.; Pecharapa, W. Structural studies and photocatalytic properties of Mn and Zn co-doping on TiO₂ prepared by single step sonochemical method. *Radiat. Phys. Chem.* **2020**, *171*, 108714. [[CrossRef](#)]
29. Wattanawikkam, C.; Pecharapa, W. Sonochemical Synthesis, Characterization, and Photocatalytic Activity of Perovskite ZnTiO₃ Nanopowders. *IEEE Trans. Ultrason. Ferroelectr. Freq. Control.* **2016**, *63*, 1663–1667. [[CrossRef](#)] [[PubMed](#)]
30. Wattanawikkam, C.; Kansa-Ard, T.; Pecharapa, W. X-ray absorption spectroscopy analysis and photocatalytic behavior of ZnTiO₃ nanoparticles doped with Co and Mn synthesized by sonochemical method. *Appl. Surf. Sci.* **2019**, *474*, 169–176. [[CrossRef](#)]
31. Jiang, W.; Zhang, X.; Gong, X.; Yan, F.; Zhang, Z. Sonochemical synthesis and characterization of magnetic separable Fe₃O₄-TiO₂ nanocomposites and their catalytic properties. *Int. J. Smart Nano Mater.* **2010**, *1*, 278–287. [[CrossRef](#)]
32. Miao, Y.; Zhai, Z.; Jiang, L.; Shi, Y.; Yan, Z.; Duan, D.; Zhen, K.; Wang, J. Facile and new synthesis of cobalt doped mesoporous TiO₂ with high visible-light performance. *Powder Technol.* **2014**, *266*, 365–371. [[CrossRef](#)]
33. Lee, J.Y.; Choi, J.-H. Sonochemical Synthesis of Ce-doped TiO₂ Nanostructure: A Visible-Light-Driven Photocatalyst for Degradation of Toluene and O-Xylene. *Materials* **2019**, *12*, 1265. [[CrossRef](#)]
34. Abdelraheem, W.; Patil, M.K.; Nadagouda, M.N.; Dionysiou, D.D. Hydrothermal synthesis of photoactive nitrogen- and boron-codoped TiO₂ nanoparticles for the treatment of bisphenol A in wastewater: Synthesis, photocatalytic activity, degradation byproducts and reaction pathways. *Appl. Catal. B Environ.* **2019**, *241*, 598–611. [[CrossRef](#)]
35. Abdelraheem, W.H.; Nadagouda, M.N.; Dionysiou, D.D. Solar light-assisted remediation of domestic wastewater by NB-TiO₂ nanoparticles for potable reuse. *Appl. Catal. B Environ.* **2020**, *269*, 118807. [[CrossRef](#)]
36. Peñas-Garzón, M.; Abdelraheem, W.H.; Belver, C.; Rodriguez, J.J.; Bedia, J.; Dionysiou, D.D. TiO₂-carbon microspheres as photocatalysts for effective remediation of pharmaceuticals under simulated solar light. *Sep. Purif. Technol.* **2021**, *275*, 119169. [[CrossRef](#)]